BIOCHEMISTRY
including biophysical chemistry & molecular biology

Article

pubs.acs.org/biochemistry

A LIN28-Dependent Structural Change in pre-let-7g Directly Inhibits Dicer Processing

Helen L. Lightfoot,[†,‡] Anthony Bugaut,[†] Javier Armisen,[‡,§] Nicolas J. Lehrbach,[‡,§] Eric A. Miska,*[,‡,§] and Shankar Balasubramanian*[,†,∥,⊥]

[†]Department of Chemistry, University of Cambridge, Cambridge CB2 1EW, U.K.

[‡]Wellcome Trust Cancer Research UK Gurdon Institute, University of Cambridge, The Henry Wellcome Building of Cancer and Developmental Biology, Cambridge CB2 1QN, U.K.

[§]Department of Biochemistry, University of Cambridge, Cambridge CB2 1QW, U.K.

[∥]School of Clinical Medicine, University of Cambridge, Cambridge CB2 OSP, U.K.

[⊥]Cancer Research UK, Cambridge Research Institute, Li Ka Shing Centre, Cambridge CB2 0RE, U.K.

Supporting Information

ABSTRACT: Several recent studies have provided evidence that LIN28, a cytoplasmic RNA-binding protein, inhibits the biogenesis of members of the let-7 microRNA family at the Dicer step in both mammals and *Caenorhabditis elegans*. However, the precise mechanism of inhibition is still poorly understood. Here we report on an in vitro study, which combined RNase footprinting, gel shift binding assays, and processing assays, to investigate the molecular basis and function of the interaction between the native let-7g precursor (pre-let-7g) and LIN28. We have mapped the structure of pre-let-7g and identified some regions of the terminal loop of pre-let-7g that physically interact with LIN28. We have also identified a conformational change upon LIN28 binding that results in the unwinding of an otherwise double-stranded region at the Dicer processing site of pre-let-7g. Furthermore, we showed that a mutant pre-let-7g that displays an open upper stem inhibited pre-let-7g Dicer processing to the same extent as LIN28. The data support a mechanism by which LIN28 can directly inhibit let-7g biogenesis at the Dicer processing step.

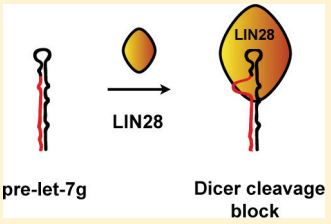

MicroRNAs (miRNAs) are small single-stranded ∼22-nucleotide RNAs that play important roles in post-transcriptional gene regulation.[1,2] miRNAs are the products of a multistep processing pathway that begins with the transcription of a long primary transcript termed the pri-miRNA. The pri-miRNA transcript is then cleaved in the nucleus by the RNase III enzyme complex Drosha-Pasha/DGCR8, which releases an ∼80-nucleotide RNA hairpin termed the pre-miRNA. The pre-miRNA is subsequently exported from the nucleus to the cytoplasm where it is processed by a second RNase III enzyme, called Dicer, to release a small RNA duplex. One strand of this duplex, the miRNA, is incorporated into an RNA-induced silencing complex (RISC) and directs the RISC complex to target mRNA (mRNA) molecules triggering their degradation and/or translational repression. miRNA expression can be regulated at both transcriptional and post-transcriptional levels.[3]

miRNAs were first characterized in *Caenorhabditis elegans* as regulators of developmental timing. The miRNAs let-7 and lin-4 were shown to be essential in the control of temporal cell fates during larval development.[4] Since then, hundreds of miRNAs have been identified, not only in *C. elegans* but also in plants and animals, including mammals. These miRNAs are involved in a variety of physiological processes, such as development, apoptosis, and carcinogenesis.[5,6]

Both the sequence and temporal expression patterns of the let-7 miRNAs are conserved from *C. elegans* to mammals.[7,8] In mammals, there are 10 members of the let-7 miRNA family. Members of the let-7 miRNA family are thought to control stem cell differentiation and developmental timing.[8] In addition, the let-7 miRNAs also function as tumor suppressors through the silencing of key oncogenes, including RAS, HMGA2, and c-MYC.[9−11]

Recently, the expression of specific members of the let-7 family has been shown to be post-transcriptionally regulated by LIN28, a cytoplasmic RNA binding protein conserved in mammals and *C. elegans*.[12−15] LIN28 contains two RNA-binding domains: a cold shock domain (CSD) and a retroviral-type CCHC zinc finger domain (ZFD). In mammals, LIN28 is expressed in embryonic stem cells (ESC) and developing tissues.[16] LIN28 has been shown to block the biogenesis of let-7 miRNAs at both the Drosha step[13,14] and the Dicer step in mammalian cells.[12,17] This regulation is mediated via a direct interaction between the LIN28 protein and the let-7 precursor RNA. In mammals, mutagenesis and competitor studies have been used to investigate the regions of the let-7 precursor that

Received: June 2, 2011
Revised: July 29, 2011
Published: August 4, 2011

is required for LIN28 binding and processing inhibition. These studies have produced conflicting evidence about the importance of the pre-let-7 terminal loop for LIN28-mediated inhibition.[12,13,18]

Undifferentiated, highly aggressive, radio-resistant tumors have been associated with a reduced level of expression of specific miRNA let-7 family members,[19,20] and it has been proposed that this could be due to the upregulation of LIN28.[21] LIN28 activation occurs in many different tumor types with a frequency of 15%, all of which are poorly differentiated tumors carrying the worst prognosis.[22] Elucidation of the molecular and mechanistic details of how LIN28 inhibits the processing of let-7 miRNAs could be essential for improving our understanding of how its misregulation can contribute to the most severe cancers and its potential as a new therapeutic target.

Here we describe the use of in vitro RNA structural mapping experiments to study the interaction of LIN28 with pre-let-7g, one of the let-7 family members most responsive to LIN28 overexpression and knockdown studies,[13] at the molecular level, and Dicer processing assays to establish its biological function.

MATERIALS AND METHODS

In Vitro Transcription Using α-^{32}P. A reaction mixture of dsDNA oligonucleotides [T7 promoter, 1 μg/μL (Table S1 of the Supporting Information)], NTPs (1 μL, 5 M CTP, GTP, and ATP, and 1 M UTP), 10× transcription buffer (Ambion, 1 μL), and uridine 5′-[α-^{32}P]triphosphate (Perkin-Elmer) was prepared. RNA polymerase (20 units) was added and the resulting mixture heated (40 °C, 1 h). TE (pH 8, 80 μL) was added, and the RNA was purified by phenol/chloroform extraction followed by a MicroSpin G-50 column (Ambion) and finally precipitated with ethanol. The extent of α-^{32}P incorporation (counts per minute) was measured using an LS 6500 multipurpose scintillation counter (Beckman Coulter).

Electromobility Shift Assay (EMSA). In vitro-transcribed [α-^{32}P]RNA (2.5×10^4 cpm) was incubated with increasing amounts of recombinant LIN28 for 45 min at room temperature (RT) in a binding buffer containing Tris-HCl (pH 7.6, 50 mM), NaCl (100 mM), β-mercaptoethanol (0.07%), $Mg(OAc)_2$ (1 mM), and total yeast RNA (12.5 μg). Glycerol (50%, 2 μL) was added, and protein−RNA complex band shifts were observed using 5% nondenaturing polyacrylamide gel electrophoresis (PAGE). The band intensities of three independent experiments were quantified using imageQuant and used to calculate the average proportion of the complex formed at each concentration of LIN28 (fraction bound). Dissociation constants (K_d) were derived from data point fitting with Origin 7.5 (OriginLab), according to the hyperbolic function $B = (B_{max}[\text{protein}])/([\text{protein}] + K_d)$, where B is the average proportion of the complex, B_{max} is the maximal amount of the complex formed, and [protein] is the total concentration of the protein.

Enzymatic Probing and Footprinting. 5′-^{32}P-labeled synthetic RNA (Table S2 of the Supporting Information) was partially digested with a combination of RNase T1, A, V1, and I (Ambion) in the presence and absence of LIN28. Labeled RNA (±LIN28) was mixed with 0.1 unit of RNase T1, 0.1 unit of RNase V1, 0.05 unit of RNase A, or 0.5 unit of RNase I with 5 μg of total yeast RNA in reaction buffer [10 mM Tris (pH 7), 100 mM KCl, and 10 mM $MgCl_2$] and incubated at RT for 15 min (A, T1, and V1) or 37 °C for 3 min (I). The cleavage reactions were stopped by ethanol precipitation. The RNA was purified by phenol/chloroform extraction followed by overnight precipitation. For an alkaline ladder, 5′-^{32}P-labeled pre-miRNA was hydrolyzed in 4 μL of an alkaline solution [50 mM sodium carbonate ($NaHCO_3/Na_2CO_3$) (pH 9.2) and 1 mM EDTA] by being heated at 90 °C for 7.5 min with 1 μg of carrier total yeast RNA. For the RNase T1 sequencing ladder, 5′-^{32}P-labeled pre-miRNA was heated at 50 °C for 5 min in denaturing buffer [20 mM sodium citrate (pH 5), 1 mM EDTA, and 7 M urea]. RNase T1 (0.5 unit) was then added and the reaction mixture incubated for a further 15 min at 50 °C. Digested products were resolved by 20% denaturing (8 M urea) PAGE and visualized by autoradiography. Cleavage bands were quantified using imageQuant and normalized against the total lane radioactivity.

Recombinant Protein Expression. LIN28 (Table S3 of the Supporting Information) and GST were subcloned into pDEST-GEX-2TK (Gateway cassette inserted at the *Sma*I site in pGEX-2TK). The recombinant proteins were expressed and purified as described previously.[15]

Dicer Processing Assay. Each reaction mixture contained 10 ng of end-labeled 5′-[^{32}P]pre-miRNA (Table S2 of the Supporting Information) and 0.1 unit of Dicer (Invitrogen) in 10 μL of 1× Dicer buffer (Invitrogen). For the protection assay, LIN28 (2 μM) was incubated with the labeled RNA at room temperature for 45 min before Dicer was added. After incubation at 37 °C for 5 min, reactions were stopped by the addition of 2× sample buffer (98% formamide, 10 mM EDTA, and 0.1% bromophenol blue) and put on ice. The RNA was resolved on a 20% denaturing gel and visualized by autoradiography. Cleavage bands were quantified from three independent experiments using imageQuant. To quantify the data in Figure 5b, we used "relative Dicer processing efficiency", which is defined as the product intensity divided by the total (products and full-length substrate) intensity.

RESULTS

The Loop Region of Human pre-let-7g Is the Sole Region Interacting Directly with Human LIN28. We first used enzymatic footprinting experiments with ribonuclease (RNase) enzymes to investigate the secondary structure of human pre-let-7g RNA. A range of different RNase enzymes with alternate sequence and/or structural specificities was chosen. We employed RNase T1, which preferentially cleaves single-stranded RNA after guanine residues; RNase A, which cleaves single-stranded RNA after the pyrimidines cytosine and uridine; and RNase V1, which is a non-sequence specific double-stranded RNA cleaving enzyme. Overall, the enzymatic digestion of pre-let-7g yielded a cleavage profile that is in good agreement with that of one of the high-energy secondary structures predicted by the RNA folding software mFOLD (Figure 1a,b). An exception was C41, a residue in the tetraloop (A40−C43) whose susceptibility to RNase A cleavage was lower than expected (Figure 1a, expanded image, lane 4). It is possible that the proximity of the bases in this constrained small loop favored stacking interactions that confer some double-stranded characteristics. In contrast, the adjacent residue, C42, also in the tetraloop, was strongly cleaved by RNase A (Figure 1a, expanded image, lane 4). In general, the cleavage patterns produced by RNases V1, A, and T1 were distinct (Figure 1a, lanes 3−5, and Figure 1b). In cases where common cleavage sites were observed, such as U23 (compare lanes 4 and 5 in Figure 1a),

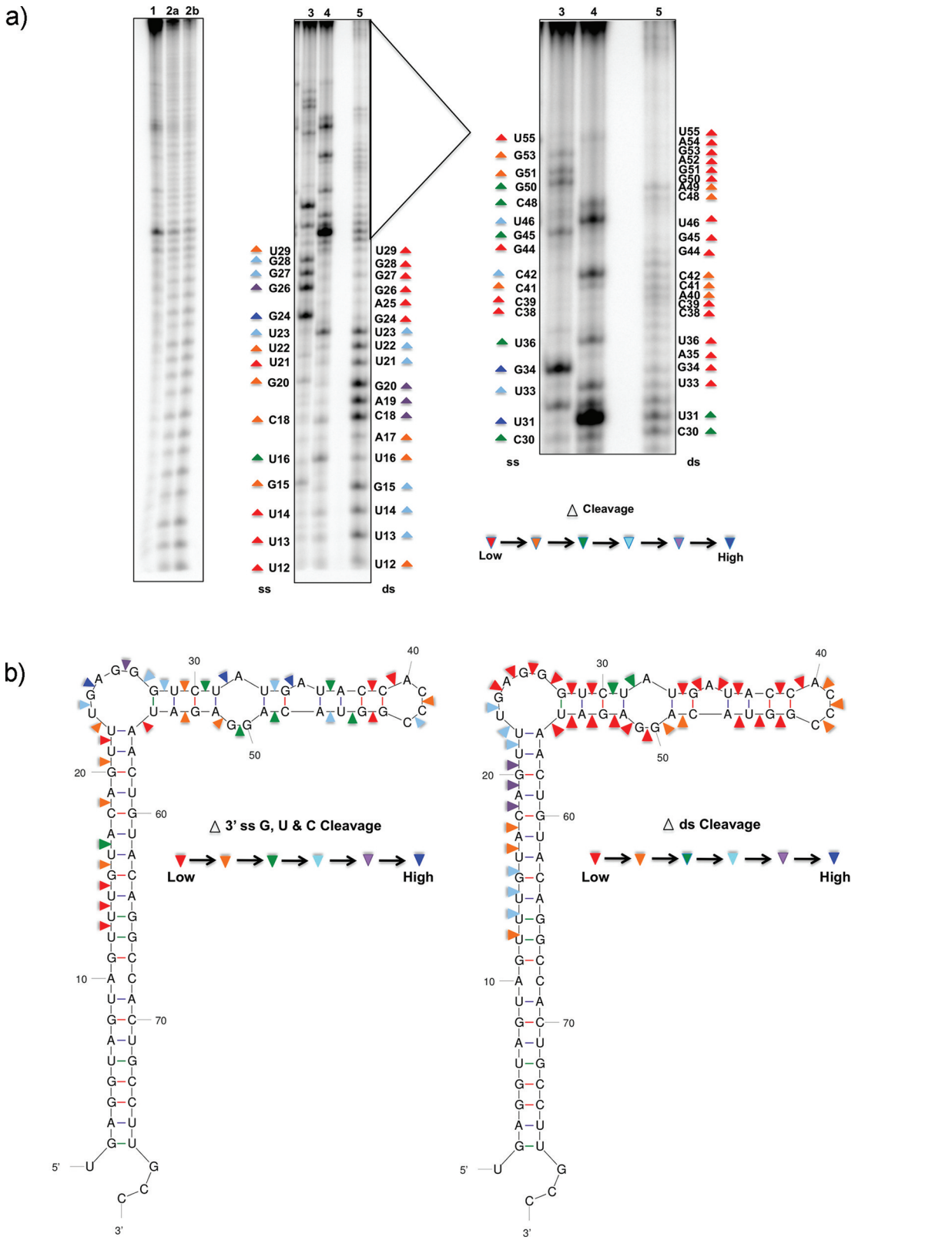

Figure 1. Enzymatic structural probing of pre-let-7g with RNase T1, RNase A, and RNase V1. (a) Representative autoradiogram of the enzymatic structural probing: lane 1, pre-let-7g; lanes 2a and 2b, pre-let-7g hydrolysis ladder; lane 3, pre-let-7g and RNase T1; lane 4, pre-let-7g and RNase A; lane 5, pre-let-7g and RNase V1. At the right is an expansion of lanes 3–5. ds means double-stranded and ss single-stranded. (b) Secondary structure of pre-let-7g based on the data from the enzymatic structural probing experiments. The colored triangles indicate the extent of nuclease-induced cleavage at various sites. The purple and red bonds represent Watson–Crick base pairing between adenine and uracil and between guanine and cytosine, respectively. The green bonds represent non-Watson–Crick base pairing between guanine and uracil.

dx.doi.org/10.1021/bi200851d | *Biochemistry* 2011, 50, 7514–7521

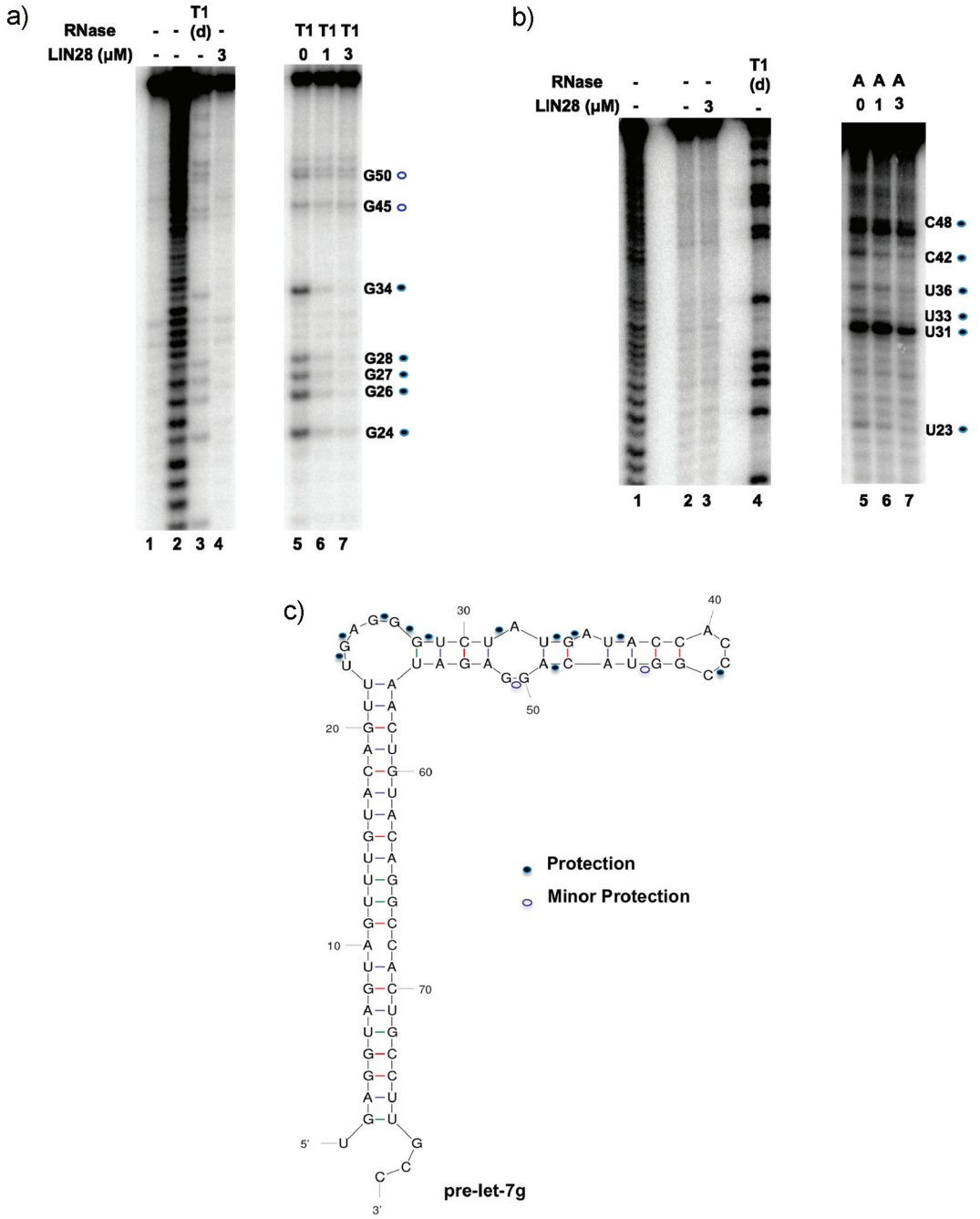

Figure 2. Enzymatic structural probing of pre-let-7g in the presence of LIN28. (a) Representative autoradiogram of the RNase T1 footprinting of pre-let-7g in the presence LIN28: lane 1, pre-let-7g; lane 2, pre-let-7g hydrolysis ladder; lane 3, pre-let-7g and RNase T1 sequencing ladder; lane 4, pre-let-7g and LIN28 (3 μM); lane 5, pre-let-7g and RNase T1; lane 6, pre-let-7g, RNase T1, and LIN28 (1 μM); lane 7, pre-let-7g, RNase T1, and LIN28 (3 μM). (b) Representative autoradiogram of the RNase A footprinting of pre-let-7g in the presence LIN28: lane 1, pre-let-7g hydrolysis ladder; lane 2, pre-let-7g; lane 3, pre-let-7g and LIN28 (3 μM); lane 4, pre-let-7g and RNase T1 sequencing ladder; lane 5, pre-let-7g and RNase A; lane 6, pre-let-7g, RNase A, and LIN28 (1 μM); lane 7, pre-let-7g, RNase A, and LIN28 (3 μM). Filled blue circles denote highly reduced levels of RNase cleavage and blue circles minor reductions in the levels of RNase cleavage. (d) denotes denaturing conditions. (c) Secondary structure of pre-let-7g summarizing the experimental data from the footprinting experiments in the presence of LIN28.

it is likely that these residues have a stacked conformation and hence have characteristics that are between those of the single-stranded and double-stranded conformations or there could be dynamic interconversion between such states. Notably, U23 is located at the junction between a stem and a bulge (Figure 1b) and could possibly be involved in stacking interactions with the terminal residues of the helical stem.

We also performed an electromobility shift assay (EMSA) to show that a glutathione *S*-transferase (GST)-tagged recombinant human LIN28 (LIN28) binds directly to pre-let-7g with a K_d value of 0.88 ± 0.22 μM (Figure S1a,b of the Supporting Information), in good agreement with a previous study using a histidine-tagged mouse LIN28 (K_d = 2.1 μM).[18] The GST tag alone did not bind to pre-let-7g (Figure S1c of the Supporting Information).

dx.doi.org/10.1021/bi200851d | *Biochemistry* 2011, 50, 7514–7521

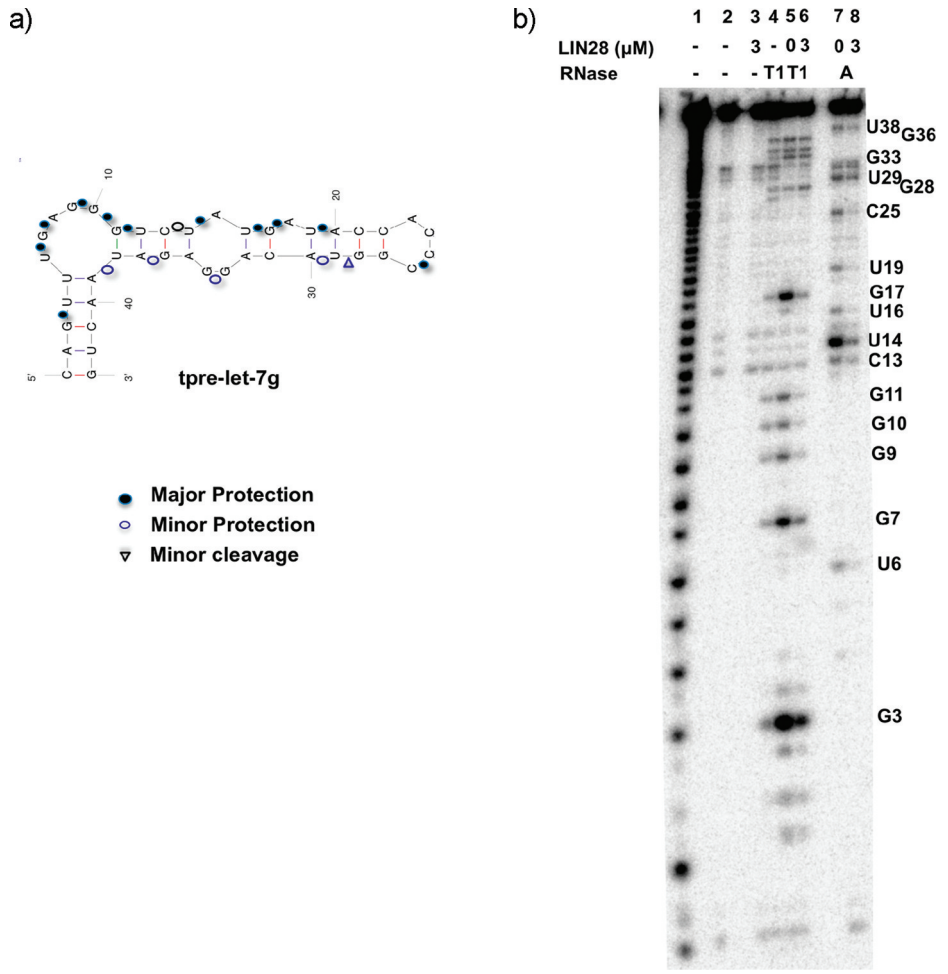

Figure 3. Enzymatic probing of tpre-let-7g in the absence and presence of LIN28. (a) Secondary structure of tpre-let-7g summarizing the experimental data from the LIN28 footprinting analysis. Filled blue circles denote highly reduced levels of RNase cleavage, blue circles minor reductions in the levels of RNase cleavage, and triangles increased levels of cleavage. (b) Representative autoradiogram of the enzymatic footprinting of tpre-let-7g in the absence and presence of LIN28: lane 1, tpre-let-7g hydrolysis ladder; lane 2, tpre-let-7g; lane 3, tpre-let-7g and LIN28 (3 μM); lane 4, tpre-let-7g and RNase T1 sequencing ladder; lane 5, tpre-let-7g and RNase T1; lane 6, tpre-let-7g, RNase T1, and LIN28 (3 μM); lane 7, tpre-let-7g and RNase A; lane 8, tpre-let-7g, RNase A, and LIN28 (3 μM).

Next, we conducted RNase T1 and RNase A enzymatic footprinting of pre-let-7g in the presence of LIN28. Enzymatic footprinting can be used to identify protein binding sites and also RNA conformational changes that are induced upon protein binding. Concentrations of protein were set at about (1 μM) and above (3 μM) the K_d value determined by the EMSA. The footprinting pattern of the terminal loop of pre-let-7g significantly changed upon LIN28 binding. When probing with RNase T1 [in Figure 2a, compare lanes 6 and 7 (LIN28 present) to lane 5 (LIN28 absent)], we observed a high degree of protection from enzymatic cleavage at the internal loop residues G24, G26, G27, and G28, and bulge residue G34. Less protection was also observed at residues G45 and G50. When probing with RNase A [in Figure 2b, compare lanes 6 and 7 (LIN28 present) to lane 5 (LIN28 absent)], we observed a high degree of protection from enzymatic cleavage at (i) internal loop/bulge residues U23 and U31, (ii) tetraloop residue C42, and (iii) Watson–Crick base-paired residues U33, U36, and C48.

The protection patterns observed in the presence of LIN28 using the RNase T1 and RNase A probes were consistent. (RNase A-protected residues were generally in the proximity of RNase T1-protected residues) and together identified several regions, spread across the terminal loop, that interacted with LIN28.

We next sought to determine if the pre-let-7g terminal loop, in the absence of the characteristic precursor stem, interacted with LIN28 in the same manner as full-length pre-let-7g, indicating that the pre-let-7g terminal loop alone is the sole requirement for the pre-let-7g–LIN28 interaction. Using a truncated form of pre-let-7g (tpre-let-7g), consisting of the terminal loop region with a 5 bp flanking stem, we found by an EMSA that LIN28 binds to tpre-let-7g with a K_d value of 1.1 ± 0.24 μM (Figure S2 of the Supporting Information), consistent with a previous study using mouse LIN28.[18] Furthermore, via RNase T1 and RNase A footprinting, we found LIN28 interacted with tpre-let-7g in a manner similar to that observed for the terminal loop in full-length pre-let-7g (compare Figure 3a and 2c). This suggests that no other region beyond the terminal loop of pre-let-7g is required for LIN28 binding, in agreement with previous reports that showed that the terminal loop is necessary and sufficient for interaction with LIN28.[12−14,23]

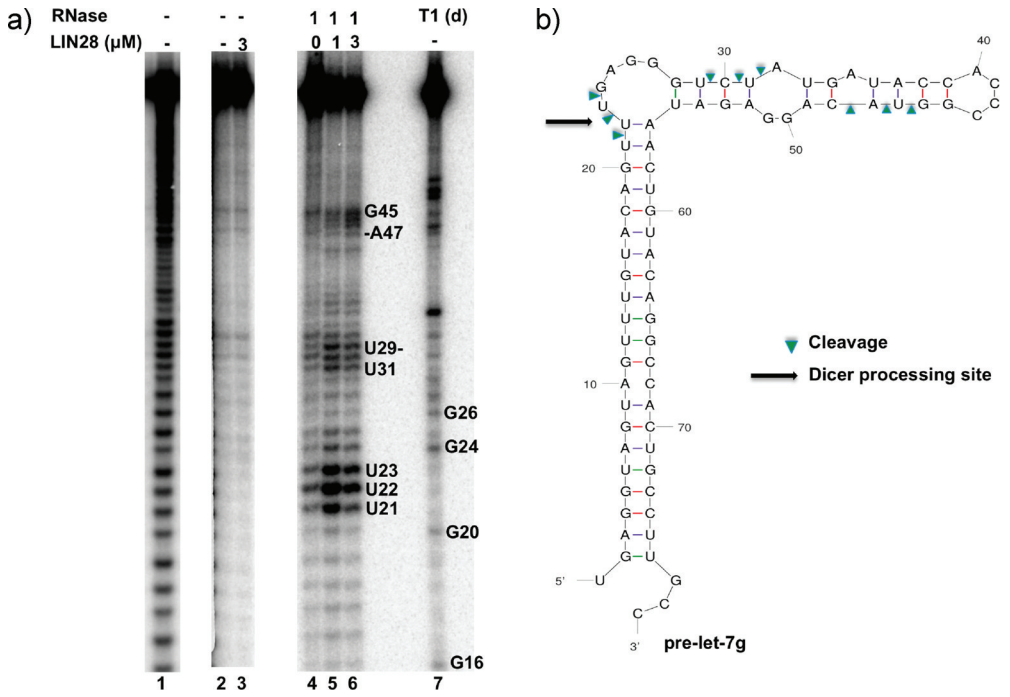

Figure 4. RNase I structural probing of pre-let-7g in the presence of LIN28. (a) Representative autoradiogram of the RNase I footprinting of pre-let-7g in the presence LIN28: lane 1, pre-let-7g hydrolysis ladder (exposure reduced relative to that of the full gel); lane 2, pre-let-7g; lane 3, pre-let-7g and LIN28 (3 μM); lane 4, pre-let-7g and RNase I; lane 5, pre-let-7g, RNase I, and LIN28 (1 μM); lane 6, pre-let-7g, RNase I, and LIN28 (3 μM); lane 7, RNase T1 ladder. (b) Secondary structure of pre-let-7g summarizing the experimental data from the RNase I footprinting experiments in the presence of LIN28.

LIN28 Binding Induces a Conformational Change in the Dicer Cleavage Site of pre-let-7g. In addition to the protection pattern described above, further enzymatic probing experiments utilizing the sequence-independent single-stranded RNase I also identified regions of increased cleavage susceptibility in the presence of LIN28. In particular, a double-stranded region (U21/U22) and the adjacent stacked base (U23) in the upper stem of pre-let-7g showed a ~2−3-fold increase in single-stranded character in the presence of LIN28 (in Figure 4a, compare lanes 5 and 6 to lane 4; quantification can be found in Figure S3 of the Supporting Information). To a lesser extent, other residues in the pre-let-7g terminal loop were also shown to have increased susceptibility to RNase I (such as U29−U31 and G45−A47) (in Figure 4a, compare lanes 5 and 6 to lane 4). Overall, our observations indicate that when LIN28 binds, conformational changes occur in the terminal loop of pre-let-7g. The conformational changes observed at residues U21−U23 predominantly result in the unwinding of the upper stem region of pre-let-7g. Interestingly, this upper stem region comprises the Dicer cleavage site (U22), and the double-stranded character of the upper stem region is thought to be essential for let-7 maturation by Dicer.[24−26]

Opening of the Upper Stem of pre-let-7g Inhibits Dicer Processing to the Same Extent as LIN28. To evaluate whether the LIN28-induced opening of the upper stem of pre-let-7g could affect Dicer processing, wild-type pre-let-7g (WTpre-let-7g), WTpre-let-7g in the presence of LIN28, and a pre-let-7g mutant with an open upper stem (MUTpre-let-7g) were tested for Dicer cleavage (Figure 5a,b) using an in vitro Dicer processing assay.[12] MUTpre-let-7g was created by mutating G20, U21, and U22 in the upper stem of WTpre-let-7g to A residues (Figure 5c). RNase VI footprinting confirmed that MUTpre-let-7g was single-stranded at the Dicer processing site (Figure S4 of the Supporting Information).

In the presence of Dicer, we observed a reduction in the amount of WTpre-let-7g and the appearance of an additional ~20-nucleotide product corresponding to mature let-7g (Figure 5a, lane 4). Upon addition of LIN28, the intensity of the mature let-7g band was reduced, indicating that LIN28 inhibits Dicer processing of WTpre-let-7g in vitro (Figure 5a, lane 6). In the absence of Dicer, LIN28 had no effect on WTpre-let-7g (Figure 5a, lane 7). For MUTpre-let-7g, the pre-let-7g mutant with an open upper stem, we found that the intensity of the mature let-7g band was greatly reduced, suggesting that the open upper stem of MUTpre-let-7g affects Dicer processing (Figure 5a, lane 5). Remarkably, we found that both the addition of LIN28 and the use of the open upper stem mutant resulted in a similar decrease, by ~65% in Dicer processing efficiency as compared to that of wild-type pre-let-7g (Figure 5b).

DISCUSSION

Using a combination of binding and enzymatic footprinting assays, we have shown that LIN28 binds to the terminal loop region of native pre-let-7g. Furthermore, we have mapped the residues of the pre-let-7g terminal loop that interact with LIN28. Overall, these data demonstrate that LIN28 binds directly to the terminal loop of pre-let-7g, in agreement with previous reports that showed that the terminal loop is necessary and sufficient for interaction with LIN28.[12−14,23] Mutagenesis studies previously indicated that some of these residues are involved in TUT4/LIN28-mediated let-7 inhibition (G50),[27] the binding of LIN28 to pre-let-7g (C42),[18] and LIN28 inhibition of let-7g processing at the Drosha step (G50).[13]

dx.doi.org/10.1021/bi200851d | Biochemistry 2011, 50, 7514−7521

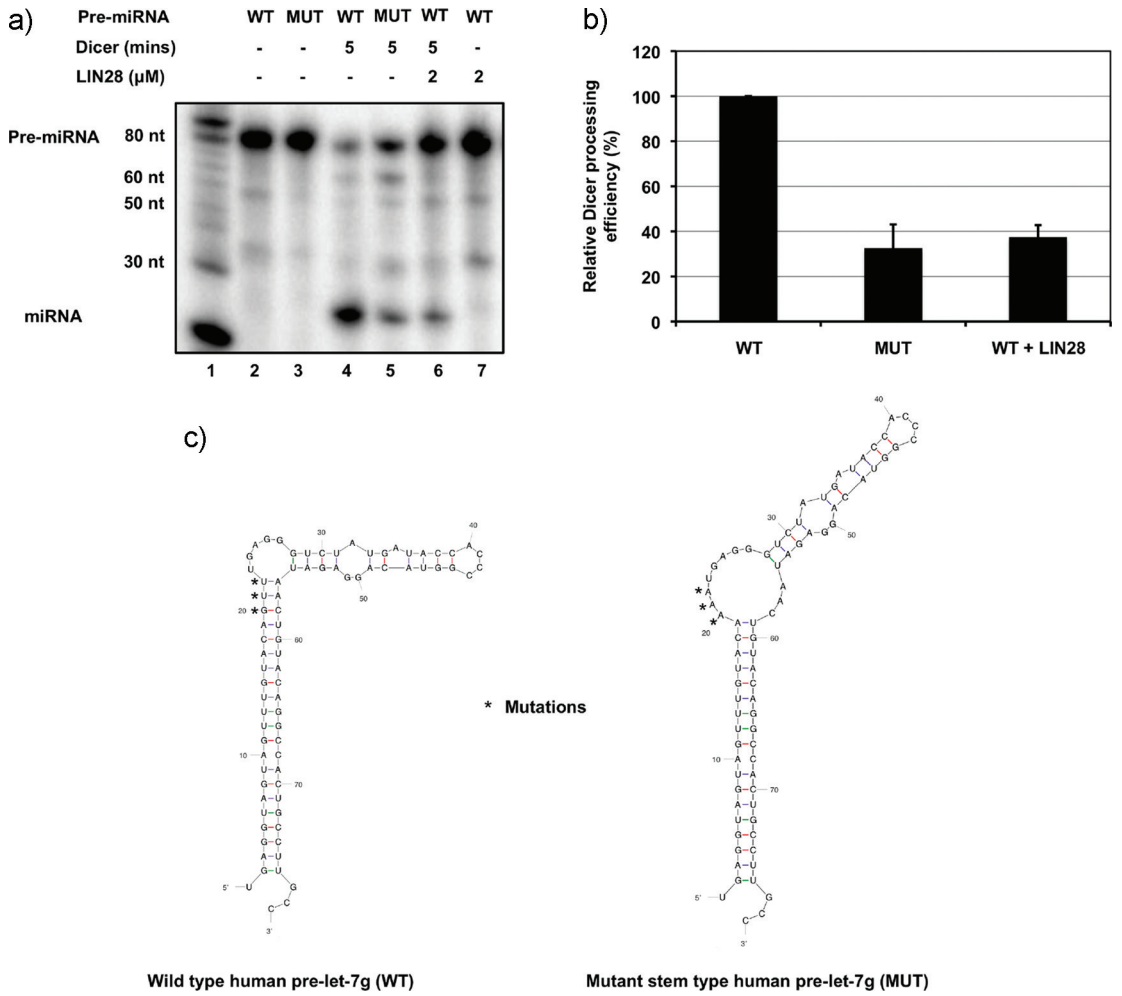

Figure 5. Dicer processing assay. (a) Representative autoradiogram of the Dicer processing assay of 5′-end-labeled wild-type pre-let-7g (WT) and mutant pre-let-7 (MUT). Dicer cleavage was allowed to proceed for 5 min. The extent of Dicer processing was quantified by calculating the relative Dicer processing efficiency, which is defined as the product intensity divided by the total (products and full-length substrate) intensity: lane 1, ladder; lane 2, WTpre-let-7g; lane 3, MUTpre-let-7g; lane 4, WTpre-let-7g and Dicer (0.1 unit); lane 5, MUTpre-let-7g and Dicer (0.1 unit); lane 6, WTpre-let-7g, Dicer (0.1 unit), and LIN28 (2 μM); lane 7, WTpre-let-7g and LIN28 (2 μM). (b) Relative Dicer processing efficiency. Results were normalized relative to the Dicer processing efficiency obtained for wild-type pre-let-7g alone, which was taken to be 100%. Error bars represent the standard deviation of three independent experiments. (c) Secondary structure of the stem mutant pre-let-7g. Mutations of wild-type pre-let-7g in the upper stem are marked with asterisks.

In addition, we have also identified a GGG motif (G26, G27, and G28) in the bulge of the pre-let-7g terminal loop that is substantially protected against nuclease cleavage upon LIN28 binding. Interestingly, this GGG motif has been demonstrated to be essential for the KH-type splicing regulatory protein (KSRP)-mediated activation of let-7 family maturation at both the Dicer and Drosha steps during differentiation of mammalian cells.[28] Altogether, our experimental data from enzymatic RNA footprinting have revealed some regions of pre-let-7g that directly interact with LIN28. However, we cannot rule out the possibility that additional points of contact could exist that were not explicitly revealed by enzymatic footprinting.

In addition, our enzymatic footprinting experiments also indicate that when LIN28 binds a conformational change occurs in the upper stem region of pre-let-7g. This conformational change results in the opening of the helix at the Dicer processing site of pre-let-7g. In the absence of LIN28, Dicer cleaves pre-let-7g at the 5′ U22 and 3′ A57 residues, releasing a dsRNA intermediate containing the 22-nucleotide mature let-7g.[29] As Dicer cleaves only dsRNA, we hypothesized that the unwinding of the upper stem region of pre-let-7g on LIN28 binding has the potential to interfere with the Dicer processing of pre-let-7g. We performed a Dicer processing assay using a mutant pre-let-7g with an open upper stem at the Dicer processing site. We found that opening of the upper stem of pre-let-7g decreases Dicer processing efficiency to the same extent (~65%) as LIN28. On the basis of these results, we can propose a model for LIN28 inhibition of let-7g biogenesis at the Dicer step, in which LIN28 binds to pre-let-7g at the terminal loop and induces a conformational change that predominately opens the helical structure of the upper stem region, reducing Dicer processing efficiency.

Several reports have demonstrated that LIN28 is able to recruit a pre-let-7 terminal uridyl transferase (TUTase).[17,23,27] The resulting 3′ polyU tail is thought to provide a signal for pre-let-7 degradation that weakens let-7 expression. Our model for a direct inhibition of pre-let-7g Dicer processing by LIN28

dx.doi.org/10.1021/bi200851d | *Biochemistry* 2011, 50, 7514–7521

might be a parallel mechanism to the recruitment of an uridylase to modify the pre-let-7 3′ end.

In conclusion, we have obtained data that provide further insights into the interaction between LIN28 and pre-let-7g. On the basis of these enzymatic in vitro studies, we propose that LIN28 could inhibit let-7g biogenesis at the Dicer step via a mechanism involving a LIN28-dependent conformational change at the Dicer processing site of pre-let-7g.

■ ASSOCIATED CONTENT

Supporting Information

Additional experimental details, data analysis, and control binding experiments. This material is available free of charge via the Internet at http://pubs.acs.org.

■ AUTHOR INFORMATION

Corresponding Author

*S.B.: telephone, +44 1223 336347; fax, +44 1223 336913; e-mail, sb10031@cam.ac.uk. E.A.M.: telephone, +44 1223 767220; fax, +44 1223 334089; e-mail, eam29@cam.ac.uk.

Funding

We thank Cancer Research UK for a Ph.D. studentship to H.L.L. and for program funding to S.B. and E.A.M. We thank the BBSRC for project funding and the Wellcome Trust for a Ph.D. studentship to N.J.L.

■ REFERENCES

(1) Carthew, R. W., and Sontheimer, E. J. (2009) Origins and Mechanisms of miRNAs and siRNAs. *Cell 136*, 642−655.

(2) Vasudevan, S., Tong, Y., and Steitz, J. A. (2007) Switching from repression to activation: microRNAs can upregulate translation. *Science 318*, 1931−1934.

(3) Bartel, D. P. (2004) MicroRNAs: Genomics, Biogenesis, Mechanism and Function. *Cell 116*, 281−297.

(4) Ambros, V., and Horvitz, H. R. (1984) Heterochronic mutants of the nematode *Caenorhabditis elegans*. *Science 226*, 409−416.

(5) Ambros, V. (2004) The functions of animal MicroRNAs. *Nature 431*, 350−355.

(6) Esquela-Kerscher, A., and Slack, F. J. (2006) Oncomirs-MicroRNAs with a role in cancer. *Nat. Rev. Cancer 6*, 259−269.

(7) Pasquinelli, A. E., Reinhart, B. J., Slack, F. J., Martindale, M. Q., Kuroda, M. I., Maller, B., Hayward, D. C., Ball, E. E., Degnan, B., Müller, P., et al. (2000) Conservation of the sequence and temporal expression of let-7 heterochronic regulatory RNA. *Nature 408*, 86−89.

(8) Roush, S., and Slack, F. J. (2008) The let-7 family of microRNA. *Trends Cell Biol. 18*, 505−516.

(9) Johnson, S. M., Grosshans, H., Shingara, J., Byrom, M., Jarvis, R., Cheng, A., Labourier, E., Reinert, K. L., Brown, D., and Slack, F. J. (2005) RAS is regulated by the let-7 microRNA family. *Cell 120*, 635−647.

(10) Lee, Y. S., and Dutta, A. (2007) The tumor suppressor microRNA let-7 represses the HMGA2 oncogene. *Genes Dev. 21*, 1025−1030.

(11) Sampson, V.B., Rong, N. H., Han, J., Jang, Q., Aris, V., Soteropoulos, P., Petrelli, N. J., Dunn, S. P., and Krueger, L. J. (2007) MicroRNA let-7a down-regulates MYC and reverts MYC-induced growth in Burkitt lymphoma cells. *Cancer Res. 67*, 9762−9770.

(12) Rybak, A., Fuchs, H., Smirnova, L., Brandt, C., Pohl, E. E., Nitsch, R., and Wulczyn, F. G. (2008) A feedback loop comprising lin-28 and let-7 controls pre-let-7 maturation during neural stem-cell commitment. *Nat. Cell Biol. 10*, 987−993.

(13) Newman, M. A., Thomson, J. M., and Hammond, S. M. (2008) Lin-28 interaction with the Let-7 precursor loop mediates regulated microRNA processing. *RNA 14*, 1539−1549.

(14) Viswanathan, S. R., Daley, G. Q., and Gregory, R. I. (2008) Selective blockage of microRNA processing by Lin28. *Science 320*, 97−100.

(15) Lehrbach, N. J., Armisen, J., Lightfoot, H. L., Murfitt, K. J., Bugaut, A., Balasubramanian, S., and Miska, E. A. (2009) LIN-28 and the poly(U) polymerase PUP-2 regulate let-7 microRNA processing in *Caenorhabditis elegans*. *Nat. Struct. Biol. 16*, 1016−1020.

(16) Moss, E. G., and Tang, L. (2003) Conservation of the heterochronic regulator Lin-28, its developmental expression and microRNA complementary sites. *Dev. Biol. 258*, 432−442.

(17) Heo, I., Joo, C., Cho, J., Ha, M., Han, J., and Kim, N. (2008) Lin28 mediates the terminal uridylation of let-7 precursor microRNA. *Cell 32*, 276−284.

(18) Piskounova, E., Viswanathan, S. R., Janas, M., LaPierre, R. J., Daley, G. Q., Sliz, P., and Gregory, R. I. (2008) Determinants of microRNA processing inhibition by the developmentally regulated RNA-binding protein Lin28. *J. Biol. Chem. 283*, 21310−21314.

(19) Weidhaas, J. B., Babar, I., Nallur, S. M., Trang, P., Roush, S., Boehm, M., Gillespie, E., and Slack, F. J. (2007) MicroRNAs as potential agents to alter resistance to cytotoxic anticancer therapy. *Cancer Res. 67*, 11111−11116.

(20) Jeong, S. H., Wu, H. G., and Park, W. Y. (2009) LIN28B confers radio-resistance through the posttranscriptional control of KRAS. *Exp. Mol. Med. 41*, 912−918.

(21) Viswanathan, S. R., and Daley, G. Q. (2010) Lin28: A microRNA regulater with a macro role. *Cell 140*, 445−449.

(22) Viswanathan, S. R., Powers, J. T., Einhorn, W., Hoshida, Y., Ng, T. L., Toffanin, S., O'Sullivan, M., Lu, J., Phillips, L. A., Lockhart, V. L., et al. (2009) Lin28 promotes transformation and is associated with advanced human malignancies. *Nat. Genet. 41*, 843−848.

(23) Hagan, J. P., Piskounova, E., and Gregory, R. I. (2009) Lin28 recruits the TUTase Zcchc11 to inhibit let-7 maturation in mouse embryonic cells. *Nat. Struct. Biol. 16*, 1021−1025.

(24) Bernstein, E., Caudy, A. A., Hammond, S. M., and Hannon, G. J. (2001) Role for a bidentate ribonuclease in the initiation step of RNA interference. *Nature 409*, 363−366.

(25) Ketting, R. F., Fischer, S. E., Bernstein, E., Sijen, T., Hannon, G. J., and Plasterk, R. H. (2001) Dicer functions in RNA interference and in synthesis of small RNA involved in developmental timing in *C. elegans*. *Genes Dev. 15*, 2654−2659.

(26) Hutvágner, G., McLachlan, J., Pasquinelli, A. E., Bálint, E., Tuschl, T., and Zamore, P. D. (2001) A cellular function for the RNA-interference enzyme Dicer in the maturation of the let-7 small temporal RNA. *Science 293*, 834−838.

(27) Heo, I., Joo, C., Kim, Y. K., Ha, M., Yoon, M. J., Cho, J., Yeom, K. H., Han, J., and Kim, N. V. (2009) TUT4 in concert with Lin28 suppresses microRNA biogenesis through pre-microRNA uridylation. *Cell 138*, 696−708.

(28) Trabucchi, M., Briata, P., Garcia-Mayoral, M., Haase, A. D., Filipowicz, W., Ramos, A., Gherzi, R., and Rosenfeld, M. G. (2009) The RNA-binding protein KSRP promotes the biogenesis of a subset of microRNAs. *Nature 459*, 1010−1014.

(29) Winter, J., Jung, S., Keller, S., Gregory, R. I., and Diederichs, S. (2009) Many roads to maturity: microRNA biogenesis pathways and their regulation. *Nat. Cell Biol. 11*, 228−234.